Article

Difference in Water CO_2 Dynamics between Riverine and Fringe Mangroves–A Case Study in Subtropical Mangroves

Wataru Nakamura [1,*], Jun Sasaki [1], Phyo Thet Naing [2], Toru Endo [3], Taiki Mori [4], Keita Furukawa [5], Kenji Ono [6] and Kiyoshi Fujimoto [7]

[1] The University of Tokyo, 5-1-5 Kashiwanoha, Kashiwa, Chiba 277-8563, Japan; jsasaki@k.u-tokyo.ac.jp
[2] Ministry of Natural Resources and Environment Conservation, Nay Phi Taw, Myanmar; phyothetnaing.mangroveforest@gmail.com
[3] Osaka Metropolitan University, 3-3-138 Sugimoto-ku, Osaka 558-8585, Japan; t.endo@omu.ac.jp
[4] Forestry and Forest Products Research Institute, 4-11-16 Kurokami, Cyuo-ku, Kumamoto, Kumamoto 860-0862, Japan; taikimori7@gmail.com
[5] Association for Shore Environment Creation, 2-4-22 Hiranuma, Nishi-ku, Yokohama, Kanagawa 220-0023, Japan; keita@meic.jp
[6] Forestry and Forest Products Research Institute, 1 Ichimatsunosato, Tsukuba, Ibaraki 305-8687, Japan; don@ffpri.affrc.go.jp
[7] Nanzan University, 18 Yamazato-cyo, Syowa-ku, Nagoya, Aichi 466-8673, Japan; kfuji@nanzan-u.ac.jp
* Correspondence: 3547103993@edu.k.u-tokyo.ac.jp; Tel.: +81-04-7136-4812

Abstract: Mangrove creeks adjoining typical riverine mangrove forests is known to be a net source of CO_2 and dissolved inorganic carbon (DIC) to the ocean due to the decomposition of rich organic carbon in the soil; such information is limited in fringe mangroves. This study aims to clarify the difference in carbonate processes between the two types of mangrove forests. We conducted continuous monitoring of the partial pressure of carbon dioxide (pCO_2) and measured carbonate chemistry parameters (total alkalinity (TA) and DIC) in two types of mangrove areas located in Okinawa, Japan. The result showed that the maximum pCO_2 reached 5242 μatm in the Fukido River estuary (a riverine mangrove), whereas it was only 765 μatm on the Yubu coast (a fringe mangrove). The measured maximum TA and DIC values were 3285 μM and 3283 μM in the Fukido River estuary and 3162 μM and 2977 μM on the Yubu coast. These indicate that pCO_2 on the Yubu coast was maintained at low values by the carbonate buffering capacity even when TA and DIC increased rapidly. The mangroves on the Yubu coast grow on dead corals and coral soils. It was suggested that the DIC/TA ratio was constantly kept at approximately 0.9 due to TA production by the dissolution of calcium carbonate ($CaCO_3$), which resulted in lower pCO_2.

Keywords: blue carbon; mangrove; tidal flat; fringe mangroves; riverine mangroves; Ishigaki Island; Iriomote Island ; Okinawa; Japan; CO_2; DIC; TA; $CaCO_3$ dissolution

1. Introduction

Coastal vegetation such as mangroves, salt marshes, and seagrasses are known as blue carbon ecosystems and are anticipated to absorb atmospheric CO_2 and store organic carbon in sediments [1]. These ecosystems are estimated to sequester carbon at a rate of approximately 31.2–82.8 Tg C yr^{-1}, with carbon sequestration within the soil on a scale of 100 to 1000 years [2]. Although blue carbon ecosystems account for only 0.2% of the ocean's surface area, they are responsible for sequestering carbon which is equivalent to about 50% of the carbon buried in ocean sediments each year [2–4]. A portion of the organic carbon buried in mangrove soils decomposes into dissolved inorganic carbon (DIC), which is subsequently outwelled into the creek through tidal pumping [5,6]. This outwelling results in an extremely high partial pressure of carbon dioxide (pCO_2) in the creek [7–10]. The high outwelling and lateral export of DIC, dissolved organic carbon (DOC), and particulate organic carbon

 doi:10.20944/preprints202306.0966.v1

(POC) from blue carbon ecosystems are expected to be stored in the ocean and are therefore considered to be a new carbon sink [11,12].

Mangroves flourish in diverse topographic and geomorphic settings characterized by periodic inundation and drying out. The macroscale framework focuses on the broad-scale geomorphological settings where climate and relative sea-level alterations come into play, and is categorized into river delta, tidal estuary, lagoon, open coast, and carbonate reef [13–16]. In terms of the global distribution of mangroves, the river delta encompasses the largest area (40.5%), followed by tidal estuary (27.5%), open coast (21.0%), and lagoon (11.0%) (carbonate reefs span all these locations) [16]. The mesoscale framework is influenced by hydrodynamics such as inundation duration, salinity, and sediment supply, and is classified as riverine, fringe, basin (interior), and overwash mangroves [15,17]. Riverine mangroves are typically found in brackish water areas, which are frequently influenced by rivers, while fringe mangroves grow along shorelines that are more affected by tides and exposed to seawater [17]. Basin (interior) mangroves are found behind fringe and riverine mangroves and are occasionally inundated by typhoons or floods [17]. Overwash mangroves grow on raised coral reefs and share a similar environment to fringe mangroves [15]. To summarize, the river delta is primarily composed of riverine and basin mangroves, while tidal estuary and lagoon are mostly formed by riverine and fringe mangroves, and open coast mainly consists of fringe mangroves. The process of outwelling and lateral export of materials from mangroves to the ocean through tidal pumping has been primarily studied through measurements taken in creeks and rivers. The outwelling of DIC from mangroves to the ocean is more dominant than that of DOC and POC [11,18].

On a global scale, the lateral exports of mangrove DIC and DOC are equivalent to 29–48% of global river inflows [11,19]. The CO_2 concentration in water is determined by the ratio of DIC to total alkalinity (TA). When the outwelling of TA surpasses DIC, the proportion of CO_2 in DIC decreases, and pH increases. Therefore, under conditions where TA is greater than DIC, the evasion of CO_2 to the atmosphere is small and most of the outwelled DIC is expected to remain in the ocean for a prolonged period [11,20]. However, these phenomena have primarily focused on the outwelling process in riverine mangroves. Compared to riverine mangroves, basin mangroves that are less exposed to tidal submergence might behave as carbon sinks [21]. Outwelling from fringe mangroves primarily takes place directly from the mangroves to the ocean, without the involvement of rivers. Nevertheless, there is a notable dearth of research on the outwelling process and water CO_2 dynamics specifically in fringe mangroves [22]. Particularly, the water CO_2 dynamics in fringe mangroves, characterized by the presence of tidal flats during low tide, may differ from those in riverine mangroves due to the suppression of outwelling. However, this process has rarely been investigated.

The rate of carbon accumulation in tidal flats is estimated to be comparable to or slightly lower than that in other vegetated coastal habitats, such as salt marshes [1,23,24]. However, our understanding of the intricacies of carbon flows on tidal flats remains limited due to various factors, including the unique biota, complex carbon fluxes, intertidal conditions, and inputs of brackish water [25]. Previous studies have examined air-water CO_2 fluxes on tidal flats using chamber and eddy covariance methods [24–27]. These investigations have revealed significant variations in air-water CO_2 fluxes influenced by factors such as light intensity, water temperature, salinity, vegetation, and benthic algae. However, there has been limited research on the variability of carbonate chemistry parameters (pCO_2, DIC, TA) specifically in tidal flats [28,29]. In particular, our understanding of the water CO_2 dynamics in tidal flats where mangroves grow landward is largely unexplored.

In this study, we hypothesize that the water CO_2 dynamics in fringe mangroves, characterized by their presence in tidal flats during low tide, differ from those observed in riverine mangroves. We postulate that these differences arise from variations in site topography and the interactions between water and sediment in these distinct environments. To test this hypothesis, we conducted field surveys in fringe and riverine mangroves that grow in the same latitudinal area, and continuously observed carbonate chemistry parameters over several tidal cycles.

Preprints (www.preprints.org) | NOT PEER-REVIEWED | Posted: 14 June 2023 doi:10.20944/preprints202306.0966.v1

2. Materials and Methods

2.1. Field sites

In this study, the Fukido River estuary in Ishigaki Island was selected as a riverine mangrove, and the Yubu coast in Iriomote Island was selected as a fringe mangrove forest (Figure 1). The Fukido River estuary is a typical riverine mangrove, which outwells carbon and nutrients to the sea through creeks during an ebb tide [30,31]. The Yubu coast exemplifies a characteristic fringe mangrove ecosystem where mangrove communities align parallel to the shoreline. During low tide, there exists an approximately 1 km expanse of tidal flat that separates the mangrove area from the adjacent ocean. These study sites are located in the subtropical region. According to the Japan Meteorological Agency, the mean temperature in summer and winter between the years 1991to 2020 were 29.1°C and 19.6°C, respectively. The mean annual precipitation during the same period was 2095 mm, with a tendency to augment during the rainy season in June and the typhoon season in September and October. These mangrove forests are inundated by high tides up to approximately 1.2 m during spring tides and are classified as micro tidal areas. The dominant mangrove species in Ishigaki Island and Iriomote Island are *Rhizophora stylosa* and *Bruguiera gymnorrhiza* [32]. Within the Fukido River estuary, *R.stylosa* was predominantly found growing alongside the creeks and in proximity to the river mouth, with *B.gymnorhiza* species growing behind them. Conversely, along the Yubu coast, the mangroves exhibit a distinct zonation pattern, with different species occurring sequentially from the seaward side to the landward side, namely *S.alba*, *R.stylosa*, and *B.gymnorhiza*, respectively (Figure 1). The maximum tree height of *R. stylosa* and *B. gymnorhiza* are 13.2 m and 11.6 m in the Fukido River estuary and 5.7 m and 11.1m along the Yubu coast, respectively [33,34].

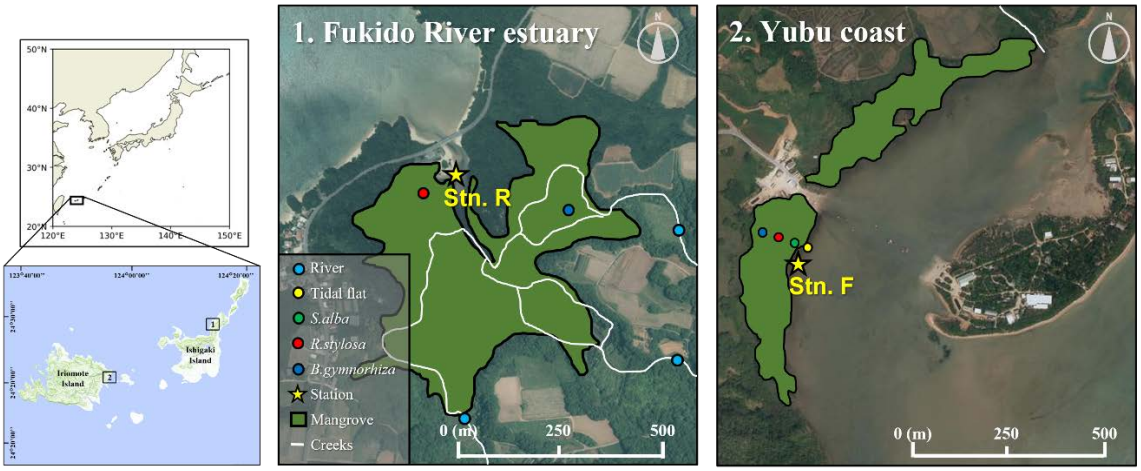

Figure 1. Field sites of this study. We selected the Fukido River estuary as a riverine mangrove, and the Yubu coast as a fringe mangrove. Yellow stars indicate the station where we installed a mooring system and collected water samples. Yellow, green, red, and blue circles indicate the site where we collected surface soil samples. The green area and white lines indicate mangrove distribution and creeks, respectively. The words R and F indicate riverine and fringe, respectively. The original pictures are from Geospatial Information Authority in Japan.

2.2. Field surveys

In the Fukido River estuary (a riverine mangrove), surveys were conducted over two separate periods: August 17-18, 2021 and August 20-22, 2022. During the 2021 survey, a platform was used to install floating water sensors in front of the mangrove forest (Stn. R in Figure 1), which were employed to record the surface water temperature, salinity, dissolved oxygen (DO), and water level. Water samples were collected at Stn. R to analyze TA, DIC, and total scale of pH (pH_T) at 1.5-hour intervals for 24 hours between August 17-18 (neap tide). To prevent biological activity, each water sample was treated with a saturated solution of mercuric chloride (10 g $HgCl_2$ per 100 mL water, 200

μL per bottle). Surface soil samples were collected from sites dominated by *R.stylosa* and stored frozen at -20°C until analysis (the red circle in Figure 1). During the 2022 survey, in addition to the floating water sensors utilized in 2021, a pCO_2 analyzer was installed (see section 2.3 Analytical Protocol). Similarly, water sampling at Stn. R for the analyses of TA, DIC, and pH_T was conducted at 2.0-hour intervals for 24 h between August 21–22 (neap tide). There was no precipitation during the surveys in the Fukido River estuary in both 2021 and 2022.

On the Yubu coast (a fringe mangrove), a survey was conducted on December 24–26, 2021. A pCO_2 analyzer and floating water sensor were attached to a platform in front of the mangrove forest (Stn. F in Figure 1) to collect pCO_2 in water and water level. Additionally, a vapor-liquid equilibrator was embedded in the soil to measure pCO_2 at a depth of 5cm (see section 2.3 Analytical Protocol). A water level sensor was also installed at a depth of 5 cm to determine the flooding conditions within the soil. Water sampling was conducted at Stn. F every 1.5 minutes over one tidal cycle on December 25 and 26 (neap tides) to analyze TA, DIC, and pH_T. During the water samplings, water temperature, salinity, and DO were also recorded. Soil cores were collected to a depth of 50 cm at a site dominated by *B.gymnorhiza*, *R.stylosa*, and *S.alba*, and surface sediment was also collected in the tidal flat (Figure 1). The survey was intermittently affected by light rainfall, and the Japan Meteorological Agency reported a total precipitation of 3.0 mm between December 24 and 26.

2.3. Analytical Protocol

The pCO_2 was measured with non-dispersive infrared (NDIR) sensors (GMP343, VAISALA Corporation, Helsinki, Finland), which were coupled with desiccant (Drierite, Thermo Scientific Chemicals, Tokyo, Japan), and an equilibrator system that was furnished with a gas-permeable membrane (PolyTetraFluoroEthylene (PTFE) tube, SUMITOMO ELECTRIC FINE POLYMER, INC., Osaka, Japan)[35]. Before conducting the field surveys, the analyzer was calibrated utilizing pure nitrogen (0 μatm CO_2) and a CO_2 span of 801 μatm (Taiyo Nippon Sanso Co., Ltd., Tokyo, Japan). The NDIR sensor exhibited an accuracy of ±10 μatm for 801 μatm of CO_2 gas at the end of each survey.

TA, DIC, and pH_T were determined using a batch-sample analyzer (ATT-05, Kimoto Electric Co., Ltd., Osaka, Japan) through the implementation of the Gran plot method [36]. A pH meter equipped with a Radiometer Analytical PHC2401-8 Combination Red-Rod pH Electrode (glass body, BNC; Product No. E16M400; Hach, Colorado, USA) was used for all analyses. The accuracies of TA and DIC were estimated to be ± 2 μM and ± 1 μM, respectively, utilizing the certified reference material (CRM) for DIC and TA (Kanso Company Ltd., Osaka, Japan).

In the Fukido River estuary, the salinity (accuracy ± 0.01), water temperature (accuracy ± 0.01 °C), and dissolved oxygen (DO) (accuracy ± 1%) at the platform were measured using a RINKO-Profiler (ASTD102, JFE Advantech, Nishinomiya, Japan). On the Yubu coast, the salinity (accuracy ± 0.1) and water temperature (accuracy ± 0.1 °C) were measured using HOBO U24-001 (ONSET, Computer Corporation, Bourne, MA, USA), and DO (accuracy ± 1%) was measured using an AAQ-RINKO (JFE Advantech). The water level (accuracy 0.4 cm) at both platforms was measured utilizing a HOBO U20L-04 (ONSET). HOBO U20L-04 was also installed inside the soil, and the inundation duration inside the soil was calculated from the pressure fluctuations.

The particle size of the surface sediments was determined using the pipette method, while the soil color was assessed by examining samples that had been dried at 110°C for 24 hours, following the guidelines provided by the Munsell soil color chart. Subsequently, the dried samples were subjected to a temperature of 550°C for 3 hours, allowing for the calculation of ignition loss based on the observed mass change. A portion of the dried samples was finely ground using a pestle and mortar, passed through a 0.5 mm mesh sieve, and treated with 1M HCl to remove inorganic carbon. Elemental composition analyses, specifically for soil organic carbon (SOC) and total nitrogen (TN), were then conducted in duplicate using an elemental analyzer (Flash EA 1112; Thermo Electron, Bremen, Germany) with a measurement involving 30-50 mg of dry sample.

To define the difference in relative ground height, we defined relative swamp height (RSH) as the elevation at which mangroves initiate inundation. The RSH, for the mean sea level (MSL), was

Preprints (www.preprints.org) | NOT PEER-REVIEWED | Posted: 14 June 2023 doi:10.20944/preprints202306.0966.v1

derived by determining the disparity between the highest recorded tidal level at the Japan Meteorological Agency Ishigaki station (located approximately 20 km away from each mangrove site) and the maximum depth measured within each mangrove swamp.

2.4. Data Analysis

The CO_2 exchange between air and water takes place in units of partial pressure (atm). pCO_2 in water is determined as follows:

$$pCO_2 = \frac{[CO_2^*]}{K_0} \quad (1)$$

where K_0 is the solubility coefficient of CO_2 and $[CO_2^*]$ is the total concentrations of CO_2 and H_2CO_3 in water. The K_0 is determined using the equation described by Weiss (1974)[37].

$$\ln K_0 = 93.4517 \times \frac{100}{T} - 60.2409 + 23.3585 \times \ln \frac{T}{100} + S\left\{0.023517 - 0.023656 \times \frac{T}{100} + 0.0047036 \times \left(\frac{T}{100}\right)^2\right\} \quad (2)$$

where T is the absolute temperature (K) and S is the salinity in parts per thousand. K_0 is influenced by temperature and salinity, and increases with decreasing water temperature. The effect of the temperature difference between the two mangrove forests on pCO_2 was calculated using the equation (1) and (2).

The observed values of TA and DIC are influenced by the mixing of freshwater and seawater and by biogeochemical processes. To analyze the variation of TA and DIC by mangrove ecosystem, normalized TA and DIC were calculated using salinity as follows [38,39]:

$$\Delta TA = \left\{\frac{TA_{obs} - TA_{S=0}}{S_{obs}}\right\} \times S_{mean} \quad (3)$$

where ΔTA is the normalized TA. TA_{obs} and is $S_{obs}$are the observed TA and salinity, respectively. $TA_{S=0}$ is the freshwater TA and S_{mean} is the mean salinity shown in Table 2. DIC was also normalized using the same equation. In the Fukido River estuary, observed values of $TA_{S=0}$ and $DIC_{S=0}$ were used ($TA_{S=0}$ = 1640 μM and $DIC_{S=0}$ =1603 μM). On the Yubu coast, $TA_{S=0}$ and $DIC_{S=0}$ were determined based on a previous report in Iriomote Island [40]. ($TA_{S=0}$ = 616 μM and $DIC_{S=0}$ =606 μM). Missing values of salinity on the Yubu coast were complemented with the mean value of each day.

Table 1. Physicochemical properties of the surface mangrove soils. SCL, S, LS. and SL indicate sandy clay loam, sand, loamy sand, and sandy loam, respectively. N.D. means no data.

Sample	Sand (%)	Silt (%)	Clay (%)	Texture	Color (dry)	SOC (%)	TN (%)	C/N	Ignition loss (%)
Fukido River estuary (A riverine mangrove). RSH is 16 ± 2 cm from MSL.									
R.stylosa	69.3	15.3	15.4	SCL	7.5 YR 3/1	6.0	0.3	26.8	13.8
B.gymnorhiza*	69.8	14.9	15.3	SCL	2.5 YR 4/2	3.1	0.1	30.2	N.D.
Yubu coast (A fringe mangrove). RSH is 34 ± 3 cm from MSL.									
Tidal flat	93.9	3.9	2.2	S	5 Y 6/2	1.1	0.04	21.5	4.1
S.alba	86.9	8.6	4.5	LS	5 Y 5/2	1.7	0.1	21.0	7.1
R.stylosa	71.4	19.3	9.3	SL	2.5 YR 3/1	4.8	0.1	41.7	25.5
B.gymnorhiza	89.1	8.0	2.9	LS	10 YR 4/1	2.7	0.1	40.0	8.0

* Data for B.gymnorhiza in the Fukido River estuary were taken from Kida et al. 2019 [41].

 doi:10.20944/preprints202306.0966.v1

Table 2. Mean values (±standard deviation) and ranges (min–max) of all parameters at Stn. R in the Fukido River estuary (a riverine mangrove) and at Stn. F in the Yubu coast (a fringe mangrove). N.D. means no data.

	pCO_2 in water (μatm)	pCO_2 in soil (μatm)	Water Temperature (°C)	Salinity	DO (%)	pH_T	TA (μM)	DIC (μM)
Fukido River estuary (A riverine mangrove)	2229 ± 1678 (657 – 5242)	N.D.	32.3 ± 2.0 (28.9 – 35.7)	33.0 ± 1.4 (29.2 – 34.1)	80.5 ± 31.5 (30.7 – 126.0)	7.772 ± 0.304 (7.226 – 8.115)	2504 ± 358 (2169 – 3333)	2365 ± 478 (1847 – 3289)
Yubu coast (A fringe mangrove)	479 ± 103 (309 – 765)	2624 ± 110 (1960 – 2831)	19.1 ± 2.5 (16.2 – 22.5)	23.9 ± 1.2 (20.5 – 25.7)	102.9 ± 4.3 (91.2 – 108.9)	7.921 ± 0.098 (7.752 – 8.082)	2827 ± 182 (2490 – 3162)	2601 ± 214 (2207 – 2977)

3. Results

3.1. Physicochemical properties of surface mangrove soils

In the Fukido River estuary, the sand content comprised less than 70% of the soil, and the surface soil texture was designated as sandy clay loam (SCL), which exhibits a considerable presence of sand and clay (Table 1). Conversely, the surface soil texture on the Yubu coast was classified as sand (S), loamy sand (LS), and sandy loam (SL), indicating a higher proportion of sand. When considering SOC concentrations in the surface soils, *R.stylosa* exhibited higher values compared to *B.gymnorhiza* in both mangrove forests. On the Yubu coast, SOC concentrations were elevated within the mangrove forest, while they were relatively lower in the seaward-growing *S.alba* and tidal flat areas.

3.2. pCO_2 and water quality change in front of each mangrove forest

In the Fukido River estuary, which is categorized as a riverine mangrove, a creek consistently extends in front of the mangrove and maintains a continuous connection to the ocean. On the Yubu coast, which is categorized as a fringe mangrove, the RSH was found to be approximately 18 cm higher compared to the Fukido River estuary. Moreover, during low tide, the mangrove and the ocean were separated by a tidal flat.

At Stn. R in the Fukido River estuary, during high tides, the inflowing seawater had a pCO_2 level of approximately 600 μatm. However, during the ebb tides, the pCO_2 level rapidly increased, and the maximum pCO_2 of the outwelled water reached 5242 μatm (Figure 2a). While, at Stn. F on the Yubu coast, during high tides, the inflowing seawater had a pCO_2 level ranging from approximately 300 to 400 μatm, and the maximum pCO_2 of the outwelled water reached 765 μatm (Figure 2d). The pCO_2 in the soil at a depth of 5 cm in Stn. F consistently remained higher than those in the air and water, ranging from 1960 to 2831 μatm (Figure 2e). When the inundated soils dried out, the aboveground pCO_2 decreased rapidly, while the pCO_2 inside the soil remained relatively stable.

Preprints (www.preprints.org) | NOT PEER-REVIEWED | Posted: 14 June 2023 doi:10.20944/preprints202306.0966.v1

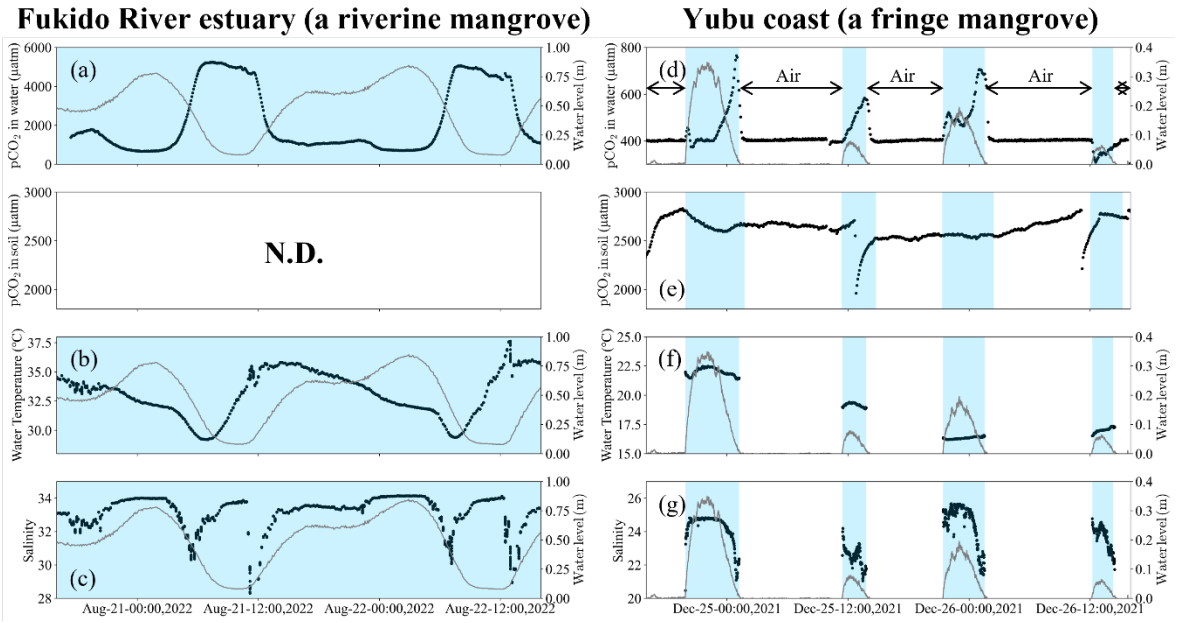

Figure 2. (a, b, c) pCO_2 in water, water temperature, and salinity change at Stn. R in the Fukido River estuary (a riverine mangrove). d, e, f, g) pCO_2 in water, pCO_2 in soil, water temperature, and salinity change at Stn. F on the Yubu coast (a fringe mangrove). Grey lines indicate water level change. Blue bands represent the duration when the platforms were inundated. N.D. means no data.

In the Fukido River estuary, the DO of the inflowed seawater was saturated (over 100%) during the flood tides and decreased to approximately 30% during the low tides (Table 1). While, on the Yubu coast, the DO remained consistently around 100% throughout the entire period. The mean water temperatures differed by approximately 13°C, with 32.3°C in the Fukido River estuary and 19.1°C on the Yubu coast (Figure 2b,f, Table 2). The standard deviation of water temperature was less than 2°C in both stations. The mean salinity was 33.0 in the Fukido River estuary and 23.9 on the Yubu coast, indicating a larger freshwater influence on the Yubu coast (Table 2). Both mangroves tended to decrease in salinity during the ebb tide (Figure 2c,g).

3.3. Carbonate parameters dynamics over several tidal cycles

The concentration and ratio of TA and DIC determine the variability in pCO_2 in water. Surface water surrounding the Yaeyama Islands in the open ocean has a TA of approximately 2250 μM and DIC of approximately 1900 μM [42,43]. At Stn R in the Fukido River estuary, the mean values of TA and DIC during high tides were 2221 μM and 1970 μM, respectively. These values are similar to those observed in the surface water around the Yaeyama Islands (Figure 3a,b, Table 1). During the ebb tides, TA and DIC concentrations increased rapidly, and the maximum TA and DIC reached 3333 μM and 3289 μM, respectively. Meanwhile, at Stn. F on the Yubu coast, the mean values of TA and DIC during high tides were 2684 μM and 2443 μM, respectively (Figure 3d,e, Table 1). These values were higher than those of the surface water around the Yaeyama Islands and Stn. R in the Fukido River estuary. The TA and DIC at Stn. F increased almost linearly from flood tides to ebb tides, and the maximum TA and DIC reached 3162 μM and 2977 μM, respectively.

Preprints (www.preprints.org) | NOT PEER-REVIEWED | Posted: 14 June 2023 doi:10.20944/preprints202306.0966.v1

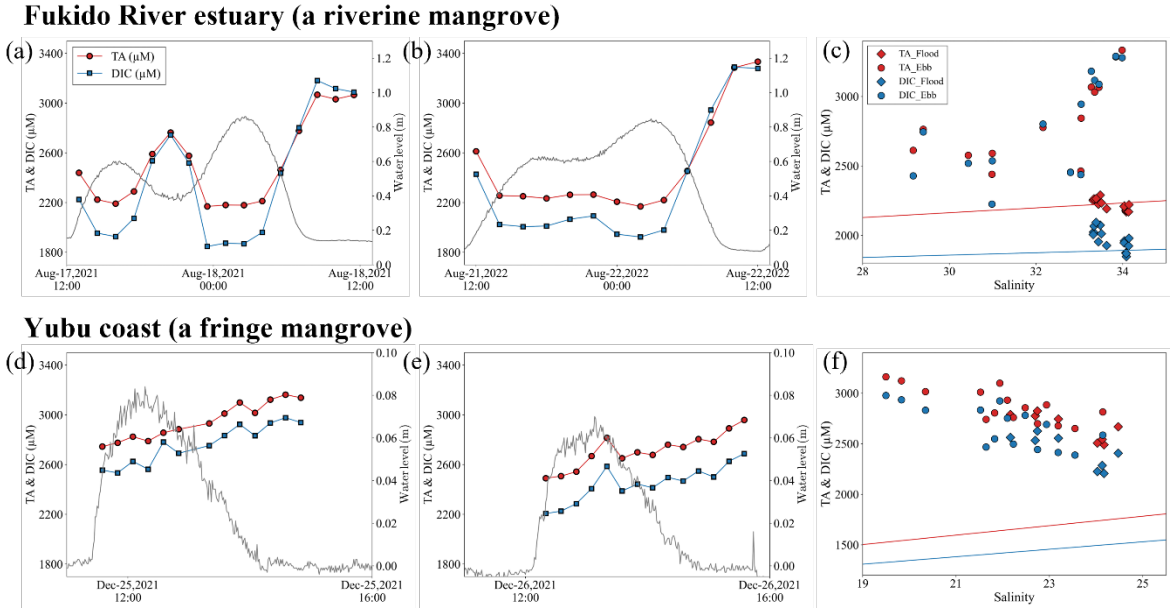

Figure 3. TA and DIC variations. a, b, c) At Stn. R in the Fukido River estuary (a riverine mangrove). d, e, f) At Stn. F in the Yubu coast (a fringe mangrove). The grey lines indicate water level change. The red and blue lines assume conservative mixing of open ocean and river water.

4. Discussion

4.1. Effect of solubility on pCO_2 dynamics

The field surveys were conducted in August 2021 and 2022 in the Fukido River estuary, and in December 2021 on the Yubu coast. The water temperatures in the two mangrove forests differed by approximately 13.2°C (Table 2). As shown in Equation 2, the solubility of CO_2 is contingent upon water temperature and salinity. Hence, it is necessary to assess the impact of disparate climatic conditions on pCO_2 dynamics. The TA and DIC values of the surface water in the open ocean around the Yaeyama Islands were documented to be roughly 2250 μM and 1900 μM, respectively, with a seasonal variation of approximately ±10 μM for both parameters [42–45]. Assuming a constant chemical composition of the open ocean water during these periods, pCO_2 was computed by altering the water temperature and salinity using the CO2SYS program [46]. The calculated pCO_2 for August 2021 and August 2022 was 384 μatm, and for December 2021, it was 169 μatm. Consequently, the impact of divergent water temperature and salinity on pCO_2 amounted to 215 μatm. Given that this study focused on pCO_2 variations exceeding 1000 μatm, the influence of water temperature and salinity on pCO_2 dynamics is anticipated to be minor.

4.2. Different impact of the geomorphic settings on pCO_2 dynamics

The Indo-Pacific region boasts the most extensive array of mangrove species and populations [32]. Okinawa, Japan, lies at the northern boundary of mangrove distribution in the Indo-Pacific region. The Yaeyama Islands in Okinawa, in particular, are the northern limit of colonization by *Rhizophora* species. *Rhizophora* species are renowned for their remarkable capacity to sequester carbon due to their abundant production of very fine roots [47]. Nevertheless, there is a dearth of research concerning the variability of carbonate chemistry parameters (pCO_2, TA, DIC) in mangrove waters within this region [40,48].

The maximum pCO_2 was 5242 μatm in the Fukido River estuary and 765 μatm on the Yubu coast (Figure 2a,b). Mangrove creeks typically exhibit pCO_2 levels exceeding 1000 μatm due to the outwelling of DIC from the soil during ebb tide [7–10]. In a creek in front of the riverine mangroves,

Preprints (www.preprints.org) | NOT PEER-REVIEWED | Posted: 14 June 2023 doi:10.20944/preprints202306.0966.v1

pCO_2 increases sharply after the mangrove soil has dried out. This phenomenon is attributed to the dilution of pCO_2 in the water by incoming seawater during the soil inundation period, which lowers pCO_2 relatively, and the outflow of aged porewater from the deeper soil layers during low tide [9], [10]. The trend of pCO_2 variation in the Fukido River estuary was comparable to that of a typical riverine mangrove; pCO_2 sharply increased after the mangrove soil dried out (Figure 2a). The rapid decrease in DO at low tide in the Fukido River estuary suggests that the soil interior was an anaerobic environment, and that decomposition was progressing (Table 2). The surface soils of the mangrove in the Fukido River estuary were identified as SCL, a soil type that would have impeded the exchange of porewater (Table 1). By contrast, on the Yubu coast, a rapid increase in pCO_2 was not observed, resulting in a much lower maximum pCO_2 compared with that in the Fukido River estuary (Figure 2b). On the Yubu coast, the mangrove forest and the ocean are separated by tidal flats at low tide. The surface soils of the tidal flat and mangrove on the Yubu coast were classified as S, LS, and SL, and exhibited a coarser grain size compared to the mangrove in the Fukido River estuary (Table 1). The consistently saturated DO levels indicated a favorable environment for porewater exchange (may not accumulated aged porewater) (Table 2).

In riverine mangroves, pCO_2 in the porewater has been reported to exceed 20,000 μatm [6]. While, on the Yubu coast, pCO_2 in the soil (porewater) was 2624 ± 110 μatm, which was only about one-tenth of that. Soil cores collected from the Yubu coast mangroves displayed a significant presence of dead coral and coral sand, with a relatively smaller amount of organic matter derived from mangroves (Figure 4). In contrast, the mangroves in the Fukido River estuary exhibited a soil texture classified as SCL, suggesting a higher deposition of mangrove-derived organic matter compared to the Yubu coast (Table 1). The Yubu coast mangrove, which developed on dead coral and coral sands with limited organic matter deposition, probably had accumulated less DIC in the soil through decomposition. On the Yubu coast, the topographic feature of being separated from the ocean at low tide inhibits porewater outwelling to the surface water, resulting in low pCO_2. Moreover, the outwelling of DIC to the ocean may have been limited at the Yubu coast compared to the Fukido River estuary.

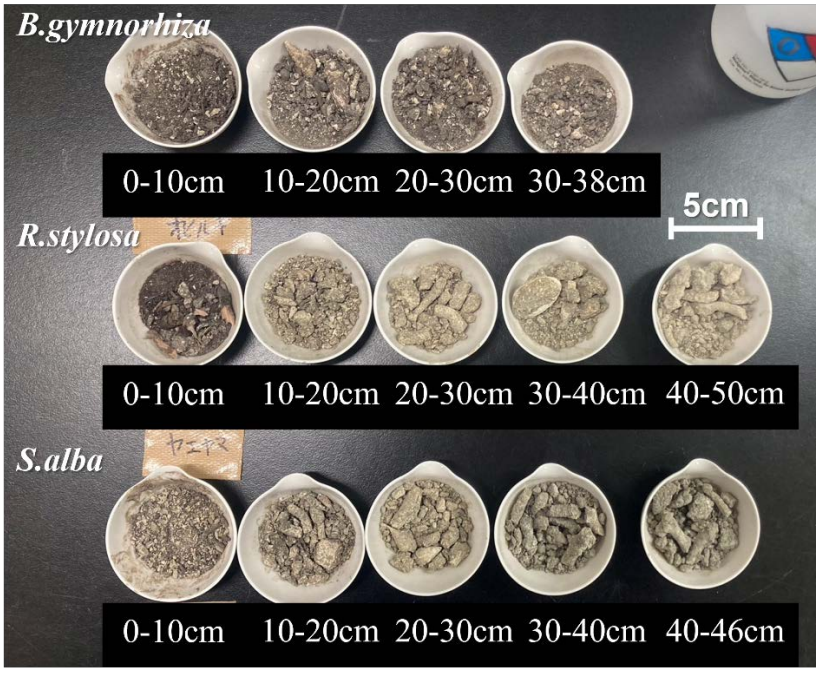

Figure 4. Dried soil samples were collected on the Yubu coast. Dead coral and coral sand were visually observed in areas where *R.stylosa* and *S.alba* were dominant.

 doi:10.20944/preprints202306.0966.v1

Fringe mangroves are predominantly found in lagoons, open coasts, and carbonate reefs [15]. These areas account for approximately 33% of all mangrove forests globally [15,16]. The study suggested that fringe mangroves, which form on coral sands and are separated by tidal flats at low tide, have a small increase in pCO_2 in the water and limited transport of material to the ocean. While the outwelling of DIC from mangroves to the ocean has been primarily investigated in creeks and rivers, additional data from fringe mangroves is needed to gain a more comprehensive understanding of the carbon cycle in mangrove ecosystems.

4.3. Geochemical impact on carbonate chemistry parameters

The concentration and ratio of TA and DIC determine the variability in pCO_2 in water. If the pCO_2 in water exceeds that in the air (approximately 400 μatm), the mangrove waters become a source of CO_2 to the atmosphere. TA represents the concentration of various alkaline substances, primarily bicarbonate (HCO_3^-), carbonate (CO_3^{2-}), and hydroxide (OH^-) ions, dissolved in the water. DIC represents the total concentration of CO_2, HCO_3^-, and CO_3^{2-} in water. Therefore, when the DIC/TA ratio exceeds 1, CO_2 in the water increases rapidly. The surface water around the Yaeyama Islands has a TA of approximately 2250 μM, DIC of approximately 1900 μM, and DIC/TA ratio of 0.84, resulting in a pCO_2 of approximately 380 μatm, making it a sink for atmospheric CO_2 [42,43]. In the Fukido River estuary, the mean values of TA and DIC during high tide were similar to those of the surface waters around the Yaeyama Islands (Figure 3c), indicating that open ocean water flows directly into the estuary without biogeochemical effects. However, on the Yubu coast, the mean TA and DIC during high tide were 2684 μM and 2443 μM, respectively, higher than those of open ocean water (Figure 3f), indicating that seawater under some biogeochemical influence was entering the Yubu coast. Tidal flats appeared during low tide on the Yubu coast, and water flowed into the mangroves by crawling on the tidal flats during flood tide. Therefore, incoming seawater on the Yubu coast may have been biogeochemically influenced by interactions with the tidal flats.

TA and DIC concentrations in mangrove waters exhibit a rapid increase due to porewater outflow affected by mineralization. The high correlation between ΔTA and ΔDIC for both mangroves indicates that the input of DIC and TA to these waters was controlled by the same process (Figure 5a). The amount of TA and DIC generated within the soil varies according to the mineralization process that contributed to the decomposition of organic carbon [49]. Among these processes, sulfate reduction has been found to have a greater impact on mangrove soils [50,51]. The variation of TA, DIC, and pCO_2 during the several tidal cycles revealed that DIC increased more than TA during ebb tides in the Fukido River estuary, and pCO_2 increased rapidly as the DIC/TA ratio increased (Figure 5b). Conversely, on the Yubu coast, TA and DIC increased during ebb tides, but the DIC/TA ratio was consistently maintained at around 0.92, and pCO_2 was below 1000 μatm (Figure 5b). This suggests that TA was produced more abundantly in the tidal flat and mangrove forest on the Yubu coast than in the Fukido River estuary, resulting in lower pCO_2. For instance, in some mangrove waters, TA and DIC variations were controlled by calcium carbonate ($CaCO_3$) dissolution, aerobic respiration, and sulfate reduction [52,53]. Furthermore, in carbonate sediment mangroves, TA was produced in abundance by the dissolution of $CaCO_3$, and a large portion of the outwelled DIC from mangroves remained in the ocean [54]. The same process may have occurred on the Yubu coast as the mangroves developed on coral sand and dean coral (Figure 4).

Preprints (www.preprints.org) | NOT PEER-REVIEWED | Posted: 14 June 2023 doi:10.20944/preprints202306.0966.v1

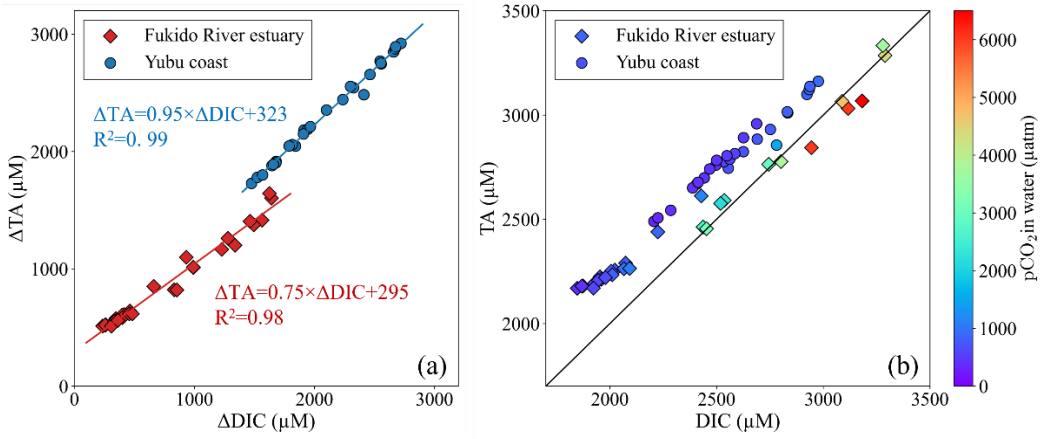

Figure 5. The relationship between TA, DIC, and pCO_2 over several tidal cycles. Diamonds and circles indicate the data in the Fukido River estuary (a riverine mangrove) and on the Yubu coast (a fringe mangrove), respectively. pCO_2 in water was calculated from DIC and TA using CO2SYS [46].

In this study, we conducted an investigation into the dynamics of pCO_2 in two mangrove forests situated at the northern distribution limit of Rhizophora species. The Fukido River estuary, characterized as a riverine mangrove, exhibited pCO_2 variations that were consistent with findings in other mangrove ecosystems (Figure 2a) [7–10]. Conversely, the mangroves on the Yubu coast, which develop on coral sand and dean coral, and are separated by tidal flats during low tide, demonstrated a limited increase in pCO_2 levels (Figure 2d). Regarding the variations in DIC and TA, high TA and DIC values were observed at Stn. F on the Yubu coast, while maintaining a relatively constant DIC/TA ratio of approximately 0.9 (Figure 5b). When the export of TA exceeds that of DIC, it is expected that DIC outwelling from mangroves to the ocean will be stored in the ocean over the long term [11]. Further investigations of mangroves growing on other reef sands will provide a more comprehensive understanding of the carbon cycle between mangroves and the ocean.

Author Contributions: Conceptualization, formal analysis, visualization, and writing—original draft preparation, W.N.; methodology, W.N. and T.E.; investigation, W.N., J.S., P.T.N, T.M., K.F., K.O., and K.F.; writing—review and editing, all authors; supervision, J.S.; funding acquisition, W.N. and K.F.. All authors have read and agreed to the published version of the manuscript.

Funding: This research was funded by the Japan Society for the Promotion of Science (KAKENHI grants 17H02034 and 21J23067).

Institutional Review Board Statement: Not applicable.

Data Availability Statement: Data available in a publicly accessible repository.

Acknowledgments: We are grateful to technical staff of Iriomote Station, Tropical Biosphere Research Center, University of the Ryukyus, for their support for our field research. Field surveys in this study were conducted with permission from the Ministry of the Environment in Japan, and Okinawa District Forest Office in Japan.

Conflicts of Interest: The authors declare no conflict of interest.

References

1. Nellemann, C.; Corcoran, E. *Blue Carbon: The Role of Healthy Oceans in Binding Carbon : A Rapid Response Assessment*; UNEP/Earthprint, 2009.
2. Howard, J.; Sutton-Grier, A.; Herr, D.; Kleypas, J.; Landis, E.; Mcleod, E.; Pidgeon, E.; Simpson, S. Clarifying the Role of Coastal and Marine Systems in Climate Mitigation. *Front. Ecol. Environ.* **2017**, *15* (1), 42–50. https://doi.org/10.1002/fee.1451.
3. Duarte, C. M.; Middelburg, J. J.; Caraco, N. Major Role of Marine Vegetation on the Oceanic Carbon Cycle. *Biogeosciences* **2005**, *2* (1), 1–8. https://doi.org/10.5194/bg-2-1-2005.

4. Duarte, C. M.; Losada, I. J.; Hendriks, I. E.; Mazarrasa, I.; Marbà, N. The Role of Coastal Plant Communities for Climate Change Mitigation and Adaptation. *Nat. Clim. Chang.* **2013**, *3* (11), 961–968. https://doi.org/10.1038/nclimate1970.
5. Stieglitz, T. C.; Clark, J. F.; Hancock, G. J. The Mangrove Pump: The Tidal Flushing of Animal Burrows in a Tropical Mangrove Forest Determined from Radionuclide Budgets. *Geochim. Cosmochim. Acta* **2013**, *102*, 12–22. https://doi.org/10.1016/j.gca.2012.10.033.
6. Chen, X.; Santos, I. R.; Call, M.; Reithmaier, G. M. S.; Maher, D.; Holloway, C.; Wadnerkar, P. D.; Gómez-Álvarez, P.; Sanders, C. J.; Li, L. The Mangrove CO2 Pump: Tidally Driven Pore-water Exchange. *Limnol. Oceanogr.* **2021**, *66* (4), 1563–1577. https://doi.org/10.1002/lno.11704.
7. Borges, A. V. Atmospheric CO2flux from Mangrove Surrounding Waters. *Geophys. Res. Lett.* **2003**, *30* (11). https://doi.org/10.1029/2003gl017143.
8. Maher, D. T.; Santos, I. R.; Golsby-Smith, L.; Gleeson, J.; Eyre, B. D. Groundwater-Derived Dissolved Inorganic and Organic Carbon Exports from a Mangrove Tidal Creek: The Missing Mangrove Carbon Sink? *Limnol. Oceanogr.* **2013**, *58* (2), 475–488. https://doi.org/10.4319/lo.2013.58.2.0475.
9. Call, M.; Maher, D. T.; Santos, I. R.; Ruiz-Halpern, S.; Mangion, P.; Sanders, C. J.; Erler, D. V.; Oakes, J. M.; Rosentreter, J.; Murray, R.; Eyre, B. D. Spatial and Temporal Variability of Carbon Dioxide and Methane Fluxes over Semi-Diurnal and Spring–Neap–Spring Timescales in a Mangrove Creek. *Geochim. Cosmochim. Acta* **2015**, *150*, 211–225. https://doi.org/10.1016/j.gca.2014.11.023.
10. Call, M.; Santos, I. R.; Dittmar, T.; de Rezende, C. E.; Asp, N. E.; Maher, D. T. High Pore-Water Derived CO2 and CH4 Emissions from a Macro-Tidal Mangrove Creek in the Amazon Region. *Geochim. Cosmochim. Acta* **2019**, *247*, 106–120. https://doi.org/10.1016/j.gca.2018.12.029.
11. Maher, D. T.; Call, M.; Santos, I. R.; Sanders, C. J. Beyond Burial: Lateral Exchange Is a Significant Atmospheric Carbon Sink in Mangrove Forests. *Biol. Lett.* **2018**, *14* (7). https://doi.org/10.1098/rsbl.2018.0200.
12. Santos, I. R.; Burdige, D. J.; Jennerjahn, T. C.; Bouillon, S.; Cabral, A.; Serrano, O.; Wernberg, T.; Filbee-Dexter, K.; Guimond, J. A.; Tamborski, J. J. The Renaissance of Odum's Outwelling Hypothesis in "Blue Carbon" Science. *Estuar. Coast. Shelf Sci.* **2021**, *255* (107361), 107361. https://doi.org/10.1016/j.ecss.2021.107361.
13. Woodroffe, C. Mangrove Sediments and Geomorphology. *Tropical mangrove ecosystems* **1992**, *41*, 7–41.
14. Twilley, R. R.; Rivera-Monroy, V. H. Ecogeomorphic Models of Nutrient Biogeochemistry for Mangrove Wetlands. *Coastal wetlands: an integrated ecosystem approach* **2009**, *1*, 641–684.
15. Woodroffe, C. D.; Rogers, K.; McKee, K. L.; Lovelock, C. E.; Mendelssohn, I. A.; Saintilan, N. Mangrove Sedimentation and Response to Relative Sea-Level Rise. *Ann. Rev. Mar. Sci.* **2016**, *8*, 243–266. https://doi.org/10.1146/annurev-marine-122414-034025.
16. Worthington, T. A.; Zu Ermgassen, P. S. E.; Friess, D. A.; Krauss, K. W.; Lovelock, C. E.; Thorley, J.; Tingey, R.; Woodroffe, C. D.; Bunting, P.; Cormier, N.; Lagomasino, D.; Lucas, R.; Murray, N. J.; Sutherland, W. J.; Spalding, M. A Global Biophysical Typology of Mangroves and Its Relevance for Ecosystem Structure and Deforestation. *Sci. Rep.* **2020**, *10* (1), 14652. https://doi.org/10.1038/s41598-020-71194-5.
17. Ewel, K.; Twilley, R.; Ong, J. Different Kinds of Mangrove Forests Provide Different Goods and Services. *Global Ecol. Biogeogr. Lett.* **1998**, *7* (1), 83–94. https://doi.org/10.1111/j.1466-8238.1998.00275.x.
18. Ray, R.; Miyajima, T.; Watanabe, A.; Yoshikai, M.; Ferrera, C. M.; Orizar, I.; Nakamura, T.; San Diego-McGlone, M. L.; Herrera, E. C.; Nadaoka, K. Dissolved and Particulate Carbon Export from a Tropical Mangrove-dominated Riverine System. *Limnol. Oceanogr.* **2021**, *66* (11), 3944–3962. https://doi.org/10.1002/lno.11934.
19. Chen, X.; Zhang, F.; Lao, Y.; Wang, X.; Du, J.; Santos, I. R. Submarine Groundwater Discharge-Derived Carbon Fluxes in Mangroves: An Important Component of Blue Carbon Budgets? *J. Geophys. Res. C: Oceans* **2018**, *123* (9), 6962–6979. https://doi.org/10.1029/2018jc014448.
20. Sippo, J. Z.; Maher, D. T.; Tait, D. R.; Holloway, C.; Santos, I. R. Are Mangroves Drivers or Buffers of Coastal Acidification? Insights from Alkalinity and Dissolved Inorganic Carbon Export Estimates across a Latitudinal Transect. *Global Biogeochem. Cycles* **2016**, *30* (5), 753–766. https://doi.org/10.1002/2015GB005324.
21. Taillardat, P.; Willemsen, P.; Marchand, C.; Friess, D. A.; Widory, D.; Baudron, P.; Truong, V. V.; Nguyễn, T.-N.; Ziegler, A. D. Assessing the Contribution of Porewater Discharge in Carbon Export and CO2 Evasion in a Mangrove Tidal Creek (Can Gio, Vietnam). *J. Hydrol.* **2018**, *563*, 303–318. https://doi.org/10.1016/j.jhydrol.2018.05.042.
22. Sippo, J. Z.; Maher, D. T.; Schulz, K. G.; Sanders, C. J.; McMahon, A.; Tucker, J.; Santos, I. R. Carbon Outwelling across the Shelf Following a Massive Mangrove Dieback in Australia: Insights from Radium Isotopes. *Geochim. Cosmochim. Acta* **2019**, *253*, 142–158. https://doi.org/10.1016/j.gca.2019.03.003.
23. Sanders, C. J.; Smoak, J. M.; Naidu, A. S.; Sanders, L. M.; Patchineelam, S. R. Organic Carbon Burial in a Mangrove Forest, Margin and Intertidal Mud Flat. *Estuar. Coast. Shelf Sci.* **2010**, *90* (3), 168–172. https://doi.org/10.1016/j.ecss.2010.08.013.

24. Otani, S.; Endo, T. CO2 Flux in Tidal Flats and Salt Marshes. In *Blue Carbon in Shallow Coastal Ecosystems: Carbon Dynamics, Policy, and Implementation*; Kuwae, T., Hori, M., Eds.; Springer Singapore: Singapore, 2019; pp 223–250. https://doi.org/10.1007/978-981-13-1295-3_8.
25. Tokoro, T.; Kuwae, T. Air-Water CO2 and Water-Sediment O2 Exchanges over a Tidal Flat in Tokyo Bay. *Frontiers in Marine Science* **2022**, *9*. https://doi.org/10.3389/fmars.2022.989270.
26. Polsenaere, P.; Lamaud, E.; Lafon, V.; Bonnefond, J.-M.; Bretel, P.; Delille, B.; Deborde, J.; Loustau, D.; Abril, G. Spatial and Temporal CO 2 Exchanges Measured by Eddy Covariance over a Temperate Intertidal Flat and Their Relationships to Net Ecosystem Production. *Biogeosciences* **2012**, *9* (1), 249–268.
27. Zemmelink, H. J.; Slagter, H. A.; van Slooten, C.; Snoek, J.; Heusinkveld, B.; Elbers, J.; Bink, N. J.; Klaassen, W.; Philippart, C. J. M.; de Baar, H. J. W. Primary Production and Eddy Correlation Measurements of CO2exchange over an Intertidal Estuary. *Geophys. Res. Lett.* **2009**, *36* (19). https://doi.org/10.1029/2009gl039285.
28. Reckhardt, A.; Beck, M.; Seidel, M.; Riedel, T.; Wehrmann, A.; Bartholomä, A.; Schnetger, B.; Dittmar, T.; Brumsack, H.-J. Carbon, Nutrient and Trace Metal Cycling in Sandy Sediments: A Comparison of High-Energy Beaches and Backbarrier Tidal Flats. *Estuar. Coast. Shelf Sci.* **2015**, *159*, 1–14. https://doi.org/10.1016/j.ecss.2015.03.025.
29. Brasse, S.; Reimer, A.; Seifert, R.; Michaelis, W. The Influence of Intertidal Mudflats on the Dissolved Inorganic Carbon and Total Alkalinity Distribution in the German Bight, Southeastern North Sea. *J. Sea Res.* **1999**, *42* (2), 93–103. https://doi.org/10.1016/S1385-1101(99)00020-9.
30. Kida, M.; Tanabe, M.; Tomotsune, M.; Yoshitake, S.; Kinjo, K.; Ohtsuka, T.; Fujitake, N. Changes in Dissolved Organic Matter Composition and Dynamics in a Subtropical Mangrove River Driven by Rainfall. *Estuar. Coast. Shelf Sci.* **2019**, *223*, 6–17. https://doi.org/10.1016/j.ecss.2019.04.029.
31. Terada, K. Rainfall Induced Water and Nutrient Fluxes at a Mangrove Estuary. *Mar. Environ. Res.* **2022**, *179*, 105674. https://doi.org/10.1016/j.marenvres.2022.105674.
32. Spalding, M. *World Atlas of Mangroves*; Routledge, 2010.
33. Ohtsuka, T.; Tomotsune, M.; Suchewaboripont, V.; Iimura, Y.; Kida, M.; Yoshitake, S.; Kondo, M.; Kinjo, K. Stand Dynamics and Aboveground Net Primary Productivity of a Mature Subtropical Mangrove Forest on Ishigaki Island, South-Western Japan. *Regional Studies in Marine Science* **2019**, *27*, 100516. https://doi.org/10.1016/j.rsma.2019.100516.
34. Fujimoto, K.; Hasada, K.; Taniguchi, S.; Furukawa, K.; Ono, K.; Watanabe, S. Progressing influences of sea-level rise to mangrove forests on Iriomote Island, southwestern Japan. Annual Meeting of the Association of Japanese Geographers, Autumn 2018. https://doi.org/10.14866/ajg.2018a.0_44
35. Endo, T.; Tanaka, T.; Otani, S.; Fujita, T.; Yamoch, S. Validity Verification of Measurement Method of Carbon Dioxide Concentration in Water using Water-resistant Breathable Tube. *Journal of Japan Society of Civil Engineers, Ser. B2 (Coastal Engineering).* **2013**, *69* (2), I_1251-I_1255. https://doi.org/10.2208/kaigan.69.I_1251.
36. Dickson, A. G.; Sabine, C. L.; Christian, J. R. *Guide to Best Practices for Ocean CO2 Measurements*; North Pacific Marine Science Organization, 2007.
37. Weiss, R. F. Carbon Dioxide in Water and Seawater: The Solubility of a Non-Ideal Gas. *Mar. Chem.* **1974**, *2* (3), 203–215. https://doi.org/10.1016/0304-4203(74)90015-2.
38. Friis, K.; Körtzinger, A.; Wallace, D. W. R. The Salinity Normalization of Marine Inorganic Carbon Chemistry Data. *Geophys. Res. Lett.* **2003**, *30* (2). https://doi.org/10.1029/2002gl015898.
39. Akhand, A.; Chanda, A.; Watanabe, K.; Das, S.; Tokoro, T.; Chakraborty, K.; Hazra, S.; Kuwae, T. Low CO2 Evasion Rate from the Mangrove-Surrounding Waters of the Sundarbans. *Biogeochemistry* **2021**, *153* (1), 95–114. https://doi.org/10.1007/s10533-021-00769-9.
40. Akhand, A.; Watanabe, K.; Chanda, A.; Tokoro, T.; Chakraborty, K.; Moki, H.; Tanaya, T.; Ghosh, J.; Kuwae, T. Lateral Carbon Fluxes and CO2 Evasion from a Subtropical Mangrove-Seagrass-Coral Continuum. *Sci. Total Environ.* **2021**, *752*, 142190. https://doi.org/10.1016/j.scitotenv.2020.142190.
41. Kida, M.; Kondo, M.; Tomotsune, M.; Kinjo, K.; Ohtsuka, T.; Fujitake, N. Molecular Composition and Decomposition Stages of Organic Matter in a Mangrove Mineral Soil with Time. *Estuar. Coast. Shelf Sci.* **2019**, *231*, 106478. https://doi.org/10.1016/j.ecss.2019.106478.
42. Chen, C. T. A.; Liu, C. T.; Pai, S. C. Variations in Oxygen, Nutrient and Carbonate Fluxes of the Kuroshio Current. *La mer 33:* **1995**, 161–176.
43. Chou, W.-C.; Sheu, D. D.; Chen, C. T. A.; Wen, L.-S.; Yang, Y.; Wei, C.-L. Transport of the South China Sea Subsurface Water Outflow and Its Influence on Carbon Chemistry of Kuroshio Waters off Southeastern Taiwan. *J. Geophys. Res.* **2007**, *112* (C12). https://doi.org/10.1029/2007jc004087.
44. Keppler, L.; Landschützer, P.; Gruber, N.; Lauvset, S. K.; Stemmler, I. Seasonal Carbon Dynamics in the Near-global Ocean. *Global Biogeochem. Cycles* **2020**, *34* (12). https://doi.org/10.1029/2020gb006571.

45. Gregor, L.; Gruber, N. OceanSODA-ETHZ: A Global Gridded Data Set of the Surface Ocean Carbonate System for Seasonal to Decadal Studies of Ocean Acidification. *Earth Syst. Sci. Data* **2021**, *13* (2), 777–808. https://doi.org/10.5194/essd-13-777-2021.
46. Humphreys, M. P.; Lewis, E. R.; Sharp, J. D.; Pierrot, D. PyCO2SYS v1.8: Marine Carbonate System Calculations in Python. *Geosci. Model Dev.* **2022**, *15* (1), 15–43. https://doi.org/10.5194/gmd-15-15-2022.
47. Ono, K.; Fujimoto, K.; Hirata, Y.; Tabuchi, R.; Taniguchi, S.; Furukawa, K.; Watanabe, S.; Suwa, R.; Lihpai, S. Estimation of Total Fine Root Production Using Continuous Inflow Methods in Tropical Mangrove Forest on Pohnpei Island, Micronesia: Fine Root Necromass Accumulation Is a Substantial Contributor to Blue Carbon Stocks. *Ecol. Res.* **2022**, *37* (1), 33–52. https://doi.org/10.1111/1440-1703.12280.
48. Ohtsuka, T.; Onishi, T.; Yoshitake, S.; Tomotsune, M.; Kida, M.; Iimura, Y.; Kondo, M.; Suchewaboripont, V.; Cao, R.; Kinjo, K.; Fujitake, N. Lateral Export of Dissolved Inorganic and Organic Carbon from a Small Mangrove Estuary with Tidal Fluctuation. *For. Trees Livelihoods* **2020**, *11* (10), 1041. https://doi.org/10.3390/f11101041.
49. Krumins, V.; Gehlen, M.; Arndt, S.; van Cappellen, P.; Regnier, P. Dissolved Inorganic Carbon and Alkalinity Fluxes from Coastal Marine Sediments: Model Estimates for Different Shelf Environments and Sensitivity to Global Change. *Biogeosci. Discuss.* **2012**, *9* (7), 8475–8539. https://doi.org/10.5194/bgd-9-8475-2012.
50. Alongi, D. M.; Pfitzner, J.; Trott, L. A.; Tirendi, F.; Dixon, P.; Klumpp, D. W. Rapid Sediment Accumulation and Microbial Mineralization in Forests of the Mangrove Kandelia Candel in the Jiulongjiang Estuary, China. *Estuar. Coast. Shelf Sci.* **2005**, *63* (4), 605–618. https://doi.org/10.1016/j.ecss.2005.01.004.
51. Kristensen, E. Carbon Balance in Mangrove Sediments: The Driving Processes and Their Controls. *Greenhouse gas and carbon balances in mangrove coastal ecosystems. Gendai Tosho* **2007**, 61–78.
52. Ho, D. T.; Ferrón, S.; Engel, V. C.; Anderson, W. T.; Swart, P. K.; Price, R. M.; Barbero, L. Dissolved Carbon Biogeochemistry and Export in Mangrove-Dominated Rivers of the Florida Everglades. *Biogeosciences* **2017**, *14* (9), 2543–2559. https://doi.org/10.5194/bg-14-2543-2017.
53. Volta, C.; Ho, D. T.; Maher, D. T.; Wanninkhof, R.; Friederich, G.; Del Castillo, C.; Dulai, H. Seasonal Variations in Dissolved Carbon Inventory and Fluxes in a Mangrove-dominated Estuary. *Global Biogeochem. Cycles* **2020**, *34* (12). https://doi.org/10.1029/2019gb006515.
54. Saderne, V.; Fusi, M.; Thomson, T.; Dunne, A.; Mahmud, F.; Roth, F.; Carvalho, S.; Duarte, C. M. Total Alkalinity Production in a Mangrove Ecosystem Reveals an Overlooked Blue Carbon Component. *Limnol. Oceanogr. Lett.* **2021**, *6* (2), 61–67. https://doi.org/10.1002/lol2.10170.